IMPERIAL

Innovative Strategies in Sustainable Formaldehyde Production in Belgium: Integrating Process Optimisation, Carbon Capture, and a comprehensive Environmental Assessment.

Soh MinChul[a] Simandjoentak Lance[a] Woldeyes Ezra[a] Yun Junhyuk[a] Qian Vanessa[a]

[a]Department of Chemical Engineering, Imperial College London, United Kingdom

ABSTRACT

A technical evaluation on the production of sustainable formaldehyde was presented in this report, including process design, advanced simulation, economic analysis, and environmental analysis. Three process configurations to produce formaldehyde were developed: a base-case with no capture of carbon, a post-combustion capture (PCC) process, which utilized 14 wt.% MEA solution-based process, and a direct air capture (DAC) route which used NaOH. Sequestered CO_2 was used as a major feedstock for methanol production via an electrocatalytic reactor (ECR), after which was converted into formaldehyde via a FORMOX process. Large-scale simulations were carried out, demonstrating a yearly methanol production capacity of approximately 62 million kilograms, with a fixed formaldehyde-to-methanol conversion ratio of 1.4 kg per kg of methanol. Economic models were developed using Aspen Process Economic Analyser, indicating that the base-case option (without capture) would involve a capital expenditure (CAPEX) of approximately $108 million and an operating expenditure (OPEX) of $427 million per year. In comparison, the PCC design was associated with a CAPEX of $120 million and a reduced OPEX of $395 million annually. The DAC option was found to require a similar CAPEX ($119 million), but a significantly higher OPEX of $519 million due primarily to the cost of reagents and electricity penalties in calcium looping. A grid-search optimisation was conducted over 10,000 data points to compare reactor geometry, with a feasible optimum identified at a diameter of 0.02 m, length of 1.00 m, at 400°C and 1 bar. Under these conditions, high selectivity in formaldehyde synthesis was achieved with very minimal side reactions, which was deemed significant as around 68% of the total CAPEX and 66% of the total OPEX were attributed to the ECR alone. Heat integration analysis using Aspen Energy Analyser was performed, and the most utilised heat exchanger (E-129) was found to manage approximately 52 million kJ/h thermal load, with a cost exceeding $841,000, reaffirming the importance of energy recovery within the design. Furthermore, a life cycle assessment (LCA) based on the ReCiPe Midpoint method was conducted, showing that the global warming potential of the reference process was around 3.90 $kgCO_{2eq}$ following process optimisation and carbon capture integration. A sustainable process design was therefore proposed, featuring a payback period of approximately 6 years and projected cumulative profits of $245 million by year 20, based on a formaldehyde base price of €2.16/kg and an ECR cost share of 20%.

Introduction

1.1. Background

Following the EU's adoption of the Paris Agreement, a net GHG emission target of 5.2 tonnes per capita by 2050 was initiated by Belgium, updating its National Energy and Climate Plan (NECP) to target a non-emission trading system (non-ETS) reduction of 42.6%, an increase from its initial target of 35% [1]. This target still remained below Europe's non-ETS mandate being misaligned with a court ruling, as Belgium's non-ETS requirement should be 55% minimum [1]. Moreover, according to the UNFCCC (United Nations Framework Convention on Climate Change) in 2022, sectorial efforts in the healthcare industry in Belgium reported to account for ~4.8% of total domestic GHG emissions. As a result, further reductions were deemed necessary [2]. Added projections indicate that GHG emissions will surge to 60% by 2050 if no interventions are made [3] This undermines the importance of sector engagement from high-impact institutions. In recognition of this, pharmaceutical leaders such as GSK have aligned with the consensus, to aim for carbon neutrality by 2030 and Net Zero by 2045 [4], [5]. However, the status quo reveals that Belgium is rapidly scaling in renewable energy deployment, to reach the ambitious climate targets. In 2024, renewables have accounted for 29.8% of electricity demand, up from 28.2% in 2023 [6]. In parallel, gas-fired electricity fell to a record low of 17.6%, reinforcing Belgium's energy resilience[7] With such changes, major investments into solar farms, offshore wind projects, and energy storage systems have appeared more attractive, with support mechanisms via EU-backed funding such as a 682 million EU package for a new offshore wind farm in Belgium [8]This scaling of solar, wind, storage, and grid integration is a deliberate strategy to provide long term viability to support Belgium's net-zero ambitions, whilst aligning with their domestic energy landscape of broader GHG and non-ETS obligations.

Recognising Belgium's commitment to achieving their climate change objectives, the department of chemical engineering at Imperial College London have produced a report to assist in that journey. A comprehensive analysis was produced, focusing on the utilisation of captured CO_2 for pharmaceutical-grade vaccine production, where conventional fossil-based fuel was substituted with Antwerp's renewable sources. The target product was a solution of industrial standard grade formalin (37–55% formaldehyde, 5-10% MeOH, and remaining H_2O by wt.%), often used as an intermediate for vaccines [9]. Formaldehyde is deemed essential in all vaccines, for its purpose in toxin inactivation [10]. According to the WHO Expert Committee and USP monograph, limits are imposed on alcohol, formaldehyde, and methanol content in a final vaccine mixture to 200 ppm [11], [12]. However, formalin is diluted prior to application in vaccines, justifying the target purity as industrial standard formalin [13].

1.2. Formaldehyde as the Key Chemical

As per **Figure 1**, the formaldehyde market is forecasted to experience imminent growth over the next four years, with a valuation projected to reach $32.72 billion by 2029, accompanied by a CAGR of 8.0% annually [14]. This growth is attributed to the increasing demand for greener infrastructure, stringent emission regulations, and its association into the healthcare and biomedical industries [14].

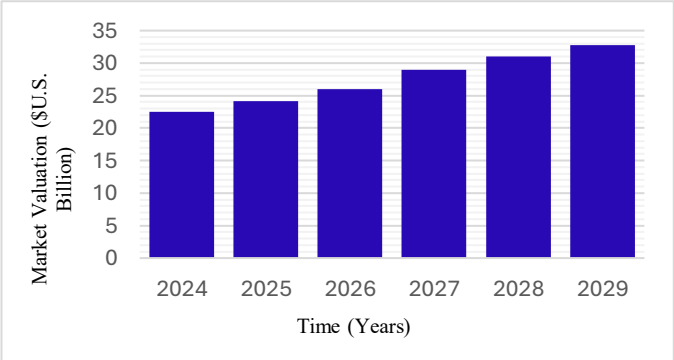

***Figure 1**: Formaldehyde Forecasted Market Growth over a 5-year market period (Adapted from the Business Research Company in 2025)*

As a result, a strong surging demand for green formaldehyde is observed, and the overarching benefit of committing research into sustainable formaldehyde production is through the preference for low-emission formaldehyde products as an alternative to be more environmentally conscious [14].

For instance, a 17% market share and a 32% annual growth rate were recorded by TheRoundUp.org, a US-based firm selling sustainable products [14]. Relative to non-sustainable product selling firms, the growth rate was found to be 2.7 times larger, indicating that more consumers were willing to remit an additional premium fee for eco-friendly brands [14].

While sustainable production methods are being established in the formaldehyde market, the compound's crucial role in the vaccine industry continues to be acknowledged. The COVID-19 pandemic was found to have spurred unprecedented attention toward inactivated vaccines, most of which relied on pathogen inactivation [15] According to the European Commission, stringent measures were proposed under the "EU Vaccine Strategy" to combat vaccine distribution inefficiencies and to enhance vaccine manufacturing and deployment capabilities [16]. By late 2021, the monthly vaccine production output in the EU was increased significantly from 20 million to 300 million doses [15] Similarly, expedited approval procedures were implemented by regulatory agencies in the USA (including the FDA and EMA), and production was scaled up through the use of parallel supply chains across different regions of the US to support formaldehyde usage in vaccines [17].

1.3. Motivation

A green formaldehyde production process was developed through an initial investigation of potential process routes, with the final selection represented by a rigorous ASPEN Plus model. The analysis of such procedure was considered vital as traditional formaldehyde production processes, via methanol (MeOH) oxidation, was associated with a high carbon footprint [18]. Building upon this motivation, the report focuses on comparing three distinct configurations of sustainable formaldehyde production: (1) without carbon capture, (2) using a post-combustion capture (PCC) process via chemical absorption (with an amine-based solvent, MEA), and (3) with an alternative carbon capture approach via direct air capture (DAC). Each configuration was assessed through economic studies, in which feasibility was determined based on CAPEX and OPEX contributions.

Various areas of the process were identified as optimisable to reduce operational and capital strain. (1) The base-case scenario was optimised through performance analyses of the reactor under various conditions. (2) The PCC process was investigated further to reduce utility costs. At a more granular level, CAPEX and OPEX reductions were targeted through the optimisation of specific components in the PCC schematic, such as the heat exchanger and reboiler. Furthermore, a computer-aided molecular design (CAMD) approach was undertaken to propose potential new solvents dedicated to CO_2 absorption, using GAMS.

To assess the viability of all three configurations, an OpenLCA simulation was conducted to evaluate the environmental impacts of each scenario using life cycle assessment (LCA) methodology to determine the most suitable long-term process for Belgium. Both environmental and economic performances were evaluated, with feasibility assessed in the context of Belgium's Net Zero targets.

2. Cradle-to-Grave Discussion

2.1. Proposed Reaction Pathway

To manufacture formaldehyde, MeOH is traditionally produced by converting natural gas into syngas by steam methane reforming (SMR) via CO_2 hydrogenation [19]. Using a conventional Cu-Zno-Al_2O_3 catalyst, the process exhibits high activity, relatively moderate selectivity, and high stability depending on the condition of the process [20]. Subsequently, MeOH is catalytically oxidised using an Ag catalyst (the BASF process) into formaldehyde and H_2O [21] However, utilising either method was not a viable option for the following reasons: (1) high energy consumption (2) high CO_2 emissions (3) potential for catalyst deactivation (4) SMR requiring a syngas feedstock [22]. In contrast, the FORMOX process is well-suited for sustainable production as it operates efficiently on CO_2-derived methanol (from captured CO_2 via electrocatalysis) and air using a robust Fe–Mo catalyst. Moreover, due to the reduced technical complexity and capital intensity of the BASF process, it is more suited for small-scale, decentralised production facilities (~5000 tons/year). Given the industrial scale required to meet Belgium's pharmaceutical and vaccine sector demands, and the reliance on low-emission feedstocks, FORMOX provides a more technically and economically viable solution. Its superior energy efficiency, higher methanol conversion and formaldehyde yields, and compatibility with CO_2-derived green methanol align with the report's overall objective of designing a low-emission, high-throughput, and cost-efficient process [23]. Therefore, the proposed reaction process exploits the electrocatalytic-reduction of CO_2 and FORMOX process for MeOH and formaldehyde production in sequence, respectively [24]. The former takes in a feed stream of captured/biogenic CO_2 and purified H_2O to produce green MeOH, as represented by the overall reaction (**R1**). This procedure was selected to exploit renewables/electricity from Belgium's energy mix, subsequently reducing atmospheric CO_2 emissions, which will be further discussed in **Section 3.2**. The exact mixture of renewables will be discussed further in **Section 2.3**. However, the essence of this ensured that employing sustainable energy sources allows for compliance with Belgium's regulations and climate objectives. The latter takes in a feed stream of MeOH to partially oxidise into formaldehyde, coupled with excess air (reaction **R2 – R6)** [25].

$$CO_2 + 2.37H_2O \rightarrow 0.66CH_3OH + 0.34CH_4 + 1.86O_2 + 0.37H_2 \quad (\mathbf{R1})$$

$$CH_3OH + 0.5O_2 \rightarrow CH_2O + H_2O \quad (\mathbf{R2})$$

$$CH_2O + 2CH_3OH \rightarrow CH_2(OCH_3)_2 \quad (\mathbf{R3})$$

$$2CH_3OH \rightarrow CH_3OCH_3 + H_2O \quad (\mathbf{R4})$$

$$CH_2O + 0.5O_2 \rightarrow H_2O + CO \quad (\mathbf{R5})$$

$$CH_3OCH_3 + O_2 \rightarrow 2CH_2O + H_2O \quad (\mathbf{R6})$$

2.2. Upstream

For all three configurations, a feedstock of CO_2 and H_2O was required to undergo the electrochemical reduction of CO_2, which was followed by subsequent conversion into formaldehyde (FA). Case 1 (without carbon capture) sourced biogenic CO_2 directly from a Stora Enso's Langerbrugge site which processes 540,000 Tonnes of recycled paper annually as a raw material [26]. The site was considered broadly self-sufficient in steam supply and 75% of its own electricity was produced from external feed waste sources, secondary streams from recycled paper production, and wind power [26]. 431,000 tonnes of biogenic CO_2 is released by Langerbrugge site (of the total 604,000 Tonnes of raw CO_2 released), and an opportunity for exploitation was thus provided [27].

In Case 2 (PCC), a conventional CO_2 chemical absorption system was used to capture high purity CO_2 which was fed into the FA production scheme. Flue gas was used as a feedstock into the absorption column, with an assumed composition of 0.191 mol % of CO_2, which was sourced directly from the RodenHuize power plant [28], [29]. As of March 2023, Belgium's largest biomass plant had been shut down due to lack of profitability, indicating its eventual decommissioning [29]. Therefore, the opportunity for flue gas utilisation for processing as a feedstock into the PCC unit was proposed by the team, relieving operational costs on the RodenHuize power plant.

Case 3 (DAC), CO_2 was sourced via direct air capture from an ambient air feed source. NaOH, a strong base, was used as a liquid solvent [30]. However, the use NaOH came with high regeneration costs from the calciner (~15 GJ/ton_{CO2}), mass transfer restrictions, and high corrosivity of the solution [30]. Regardless, this was found to undermine the strong binding affinity towards CO_2 [30]. NaOH was supplied from Vynova, a globally known distributor of caustic soda, which was provided in solution concentrations up to 50 wt% [31]. Its production site is located in Tessenderlo (Belgium); thus, logistics and distribution were not a major issue.

H_2O from Veolia's Rapide Strata Water Technology was sourced by all processes, producing high purity water using ion-exchange de-ionisers. Using nanofiltration, negatively charged ions are trapped by

this technology onto positively charged resins, resulting in highly purified water [32]. Veolia's technology guaranteed a constant supply of purified water, as the unit regeneration cycle ranged only between 30-60 minutes, with a small carbon footprint [32].

2.3. Renewable Energy Sources

According to the IEA, Belgium's energy policy is currently centralised on shifting to a low-carbon economy, ensuring energy-security, reducing consumer expenses, and maintaining fair competition in the market [33]. As a result, Belgium has made strong progress in this field, proving a leading contender in offshore wind supply [33]. Consequently, the process has explored the outcome of using a mixture of offshore wind energy and solar-PV, as these were the two most dominant sources at 19.0% in 2023 of the total generation [33]. Note that relying solely on renewables may be infeasible, due to intermittency and variability – proving inevitable shortfalls in energy supply. Subsequently, exploring alternative non-renewables such as nuclear energy was a consideration if needed to meet 'un-filled' gaps in the energy demand [34]. Overall, this validated and aligned with Belgium's goals under the EU parliament, after the 'fit for 55' revision of the Effort-sharing Regulation (ESR) – which had set Belgium's emissions reduction obligation for 2030 to 47% compared with 2005 [35]. Belgium also aims to improve energy efficiency throughout the industry sector by replacing fossil fuel resources with electrification-powered heating, confirming the validity of our approach [35].

3. Base Case Process Modelling

3.1. MeOH Production

The core reactions within the electrocatalytic reactor are reduction /oxidation processes which occurs at the cathode/anode as follows:

$$CO_2 + 6H^+ + 6e^- \rightleftharpoons CH_3OH + H_2O \quad \textbf{(R7)}$$

$$CO_2 + 8H^+ + 8e^- \rightleftharpoons CH_4 + 2H_2O \quad \textbf{(R8)}$$

$$2H^+ + 2e^- \rightleftharpoons H_2 \quad \textbf{(R9)}$$

$$2H_2O \rightleftharpoons O_2 + 4H^+ + 4e^- \quad \textbf{(R10)}$$

Direct modelling of these reactions in Aspen Plus proved infeasible due to complexities beyond Butler-Volmer simplifications and software limitations, restricting electrolysis reactions to only exhibit hydrolysis [36]. Hence, a dual-step modelling approach was employed: first, a digital twin of the methanol synthesis process was developed in GAMS to compute reaction extents ensuring steady-state. The calculated reaction extents and split fractions for splitters from the GAMS model was transferred to the Aspen model. Subsequently, a RStoic unit in Aspen Plus was utilised based on the extents. The key mathematical relations governing the electrocatalytic reactor include:

$$F_{out,i} = F_{in,i} + \sum_j \nu_{i,j}\xi_j \quad \textbf{(E2)}$$

$$I_j = \left|\nu_{e^-,j}\right|\xi_j F \quad \textbf{(E3)}$$

$$I_4 = I_1 + I_2 + I_3 \quad \textbf{(E4)}$$

$$X_{CO_2} = \frac{\xi_1+\xi_2}{F_{in,CO_2}} \quad \textbf{(E5)}$$

$$\frac{S_1}{S_2} = \frac{\xi_1}{\xi_2} \quad \textbf{(E6)}$$

$$\eta = \frac{\xi_3}{\xi_1 + \xi_2} \quad \textbf{(E7)}$$

Where $F_{k,i}$ defines the molar flowrate of species in and out of the reactor, $\nu_{i,j}$ is stoichiometric coefficient of species for each reaction, ξ_j is extent of reaction, I_j is current required by each reaction, X_{CO_2} defines the CO_2 conversion, S_1 and S_2 defines the selectivity of reaction **R7** and **R8**, η defines the faradaic efficiency towards the reaction **R9**. All parameters such as CO_2 conversion (20%), selectivity (66% and 34%), and faradaic efficiency (10%) were sourced from literature [37], [38]. Given the presence of ions and electrons in the model, dummy reactions and extents of reaction were introduced for accurate incorporation:

$$CO_2 + 2H_2O \rightleftharpoons CH_3OH + 1.5\ O_2 \quad \textbf{(R11)}$$

$$CO_2 + 2H_2O \rightleftharpoons CH_4 + 2O_2 \quad \textbf{(R12)}$$

$$H_2O \rightleftharpoons H_2 + 0.5O_2 \quad \textbf{(R13)}$$

$$F_{out,i} = F_{in,i} + \sum_j \nu'_{i,j}\xi'_j \quad \textbf{(E8)}$$

The ν' and ξ' defines the stoichiometric coefficient of dummy reaction and dummy extent of reaction. The corresponding dummy extents ensured consistency between the GAMS-calculated extents and Aspen simulations.

A key aspect of the process model was the incorporation of recycle streams, which requires steady-state operation through an appropriate separation system. Initially inspired by Luyben's work, only the flash drum operating conditions - 38°C and 106.5 bar - were directly adopted due to differences in fluid composition [39]. For the separation process design, Antoine coefficients were used where DOI; otherwise, the Clausius-Clapeyron equation was employed.

Following the flash drum, the MeOH-rich stream still contained significant CO_2, necessitating further purification through additional distillation columns. This was expected according to the high CO_2 solubility in MeOH, as shown by the experimental VLE data by Valtz et al. [40]. These columns were designed using heuristic approaches to ensure MeOH purification from MeOH-water-CO_2 system, while mass balances were computed using the GAMS model. The distillation columns in GAMS were assumed to operate under sharp split conditions. Additionally, split fractions for the splitters were treated as decision variables within the GAMS framework to ensure convergence to steady state.

Subsequently, the Aspen Plus simulation was developed using the dummy extents of reactions and split fractions, determined by GAMS. Distillation columns were implemented using RadFrac blocks, with operating conditions - feed temperature and pressure, number of stages, and reflux ratios - tuned to match recovery rates specified in the GAMS model.

According to a study, the CO_2 electrocatalytic reduction is most often reported with metal oxide electrodes [41]. Thus, the base case model assumed use of copper oxide as the electrodes. In this base case, 10% of the methanol product stream was allocated for potential commercial sale. A detailed analysis of this scenario is provided in **Section 4.2**.

3.2. Formaldehyde Production

As discussed, the FORMOX route was selected (**Figure 2**), which uses a highly stable $Fe_2(MoO_4)_3$ catalyst with a MoO_3 promoter. This catalyst allows the methanol oxidation to proceed rapidly at ~250–400 °C, achieving high conversion (~98-99%) and yield between 88 – 92% [25]. In the bargain, the Fe catalysts act as a nanometer-sized catalyst with fine particle size, creating larger surface area with catalyst active sites [42]. Trace impurities are also better tolerated than silver catalysts, which is an important factor for long-term operation.

The primary reaction is the partial oxidation (**R2**). This is accompanied by side reactions (**R3 – R6**), including further oxidation of formaldehyde to carbon monoxide and parallel reactions such as methanol dehydration to dimethyl ether (DME) and formation of dimethoxymethane (DMM) from MeOH and formaldehyde. Kinetic expressions were adapted from literature to ensure accurate reaction rate predictions. Detailed rate laws and Arrhenius parameters for Fe-Mo catalysed partial oxidation of methanol were obtained from published studies and implemented in Aspen Plus [43]. This enabled simulation of conversion and selectivity based on specified reactor dimensions and operating conditions.

In the formaldehyde section, thermodynamic property selection followed the guidance of Carlson's workflow for such mixtures, to ensure reliable vapor–liquid equilibrium predictions for the absorber and distillation [44]. Based on the mixture regime, the model chosen for the Aspen simulation was an activity coefficient model (NRTL) for liquid-phase equilibrium. This was suited to accurately model the formaldehyde–water–methanol mixture, which is highly non-ideal [44]. The formaldehyde reactor was modelled as an ideal plug flow reactor (PFR), using Aspen's RPlug model. In practice, the FORMOX

process uses a multi-tubular fixed-bed reactors: many parallel tubes packed with catalyst, housed in a shell through which heat transfer fluid circulates. This design provides a high surface area for heat removal - critical because the methanol oxidation reactions are highly exothermic.

The FORMOX reactor was designed isothermally at 400℃ and near-ambient pressure (~1 atm). Heat removal was achieved by circulating heat transfer oil around the reactor tubes to maintain the set temperature. Initial reactor dimensions were based on literature [45], and the plug flow reactor (PFR) length was adjusted to achieve high MeOH conversion with minimal by-product formation. By appropriating the reactor tube bundles to an equivalent single tube, a reactor configuration of 10 m length and 1.5 m equivalent diameter yielded ~98.2% and 89.5% MeOH conversion and yield in a single pass, respectively. Further increases in reactor length led to higher selectivity losses due to side reactions, particularly beyond 10 m. Therefore, this configuration was chosen as a trade-off between conversion and selectivity.

Hot gaseous products were then cooled via heat exchange (recovering energy for feed preheating) and passed through a flash drum, where any remaining non-condensable gases (mainly nitrogen) were removed to prevent accumulation. The remaining formaldehyde-methanol mixture entered a water-based absorption system, which captures formaldehyde and removes residual gases. A conventional water absorption approach was chosen over membrane separation due to modelling limitations in Aspen, economic uncertainties, and limited industrial validation of membranes. Water absorption remains the industry standard for reliability and simplicity reasons.

The system was modelled using a single packed absorber column (Aspen RadFrac), where the gas stream is brought into contact with a counter-current flow of deionised water. Formaldehyde, being highly soluble and forming hydrates in water, is efficiently absorbed. An excess water flow of approximately 215 kmol/h was employed to achieve over 99% formaldehyde capture and to maintain the column temperature between 50–70 °C at near-ambient pressure (~1 atm). The absorber produced a bottom stream of dilute formalin, and a vent stream primarily composed of N_2, O_2, and trace organics, which was safely purged.

The dilute formaldehyde solution (formalin) which exited the absorber contained formaldehyde, water, and residual methanol. To meet purity and stability targets, the stream was fed to a distillation column, operated under mild vacuum to prevent formaldehyde degradation. Excess water was stripped and concentrated the formaldehyde solution to ~37 wt%. The tops, consisting of mainly water, was recycled back to the absorber, whilst a fraction was purged. To stabilise the formaldehyde, ~7% of upstream methanol was diverted from the reactor and blended into the final product. **Table 1** below summarises the composition of the final formalin product.

Table 1: Final Formalin Composition (wt%)

Final formalin composition		
FA	H_2O	MeOH (Stabiliser)
44%	51.8%	4.2%

3.3. Post Combustion Capture (PCC) (Case 2)

One alternative case to CO_2 sourcing was through a PCC unit, using MEA as a chemical absorbent. A process flow diagram can be found in **Figure 2**. The design parameters (shown in **Table 2**) used in the feed streams, absorption and stripping columns were acquired from Maddedu et al. [28], incorporating lab-scale data from a study by Tontiwachwuthikul et al. [46]. The study specified an MEA composition of 14 wt%, which was used in the PCC unit for the absorption process. However, further refinement to the parameters were made to account for the scale of the process, which involved adjusting the feed flow and column sizing to produce the required CO_2 product flow of ~500 kmol/h.

The column height to diameter ratio for the absorption and stripping columns were adjusted from 65:1 and 39:1 to 4:1 as recommended by ICARUS Corporation who give a range from 3:1 to 20:1 for industrial vertical vessels [47].

Table 2 - Design data for PCC ASPEN modelling

Column Specifications		
	Absorber	Stripper
Column Height (m)	26	15.2
Column Diameter (m)	6.5	3.8
Number of Stages	30	20
Flooding Capacity (%)	68	78
Operating Temperature (°C)	32	120
Operating Pressure (bar)	1	2
Section Pressure Drop (bar)	0.087	0.029
Packing Material	Berl Saddles (13mm)	Mellapak (250Y)
HX Duty (kW)	79993	
Cooler Duty (kW)	21076	

Consistent with lab-scale data, the absorption column operating temperature was set at 32°C. Since the operating temperature depends on the amine composition, 32°C was found to achieve a CO_2 recovery rate of 99.9%. To assess the potential for improved mass transfer and reaction kinetics, the temperature was increased to 45°C. While higher temperatures can enhance absorption rates and reduce solvent circulation requirements, it was found that 45°C did not improve CO_2 recovery but required a larger column, increasing capital costs. This justified maintaining the operating temperature at 32°C to balance performance and cost. Literature recommended temperatures of both stream 'STRIN' (see **Figure 2**) and the reboiler unit (REB) to be maintained at 110°C and 120°C respectively, to prevent solvent degradation that occurs above 120-130°C *[48]*. The condenser (CON) temperature specification from *[28]* suggested 19°C, which provided a CO_2 product purity of 98%. Pipeline transport typically requires a purity of >97% to prevent CO_2 dissolution in water, which can cause corrosion *[49]*. While 19°C met this requirement, increasing the temperature to 25°C maintained 98% purity while reducing condenser utility demands. *The absorption column was kept at atmospheric pressure, while the stripper pressure was increased to 2 bar to enhance CO_2 stripping efficiency. The pressure increase raised the partial pressure of CO_2 in the gas phase, improving desorption by shifting the reaction equilibrium towards CO_2 release. Additionally, operating at 2 bar reduced water vaporisation losses, lowering steam consumption and improved energy efficiency. However, reducing the pressure back to atmospheric levels required a larger column to maintain stripping efficiency, highlighting the trade-off between equipment size and energy consumption.*

3.4. Direct Air Capture (DAC) (Case 3)

In the simplified direct air capture (DAC) process (**Figure 2**), ambient air was pumped through an air contactor, where CO_2 was absorbed using a sodium hydroxide (NaOH) solvent. The absorbed CO_2 formed sodium carbonate (Na_2CO_3), which was then transferred into a pellet reactor operating at around 25°C and atmospheric pressure (1 atm), where crystallisation occurs. In this reactor, sodium carbonate reacts with calcium hydroxide ($Ca(OH)_2$) to produce calcium carbonate ($CaCO_3$), a solid precipitate, while simultaneously regenerating the sodium hydroxide solvent [50].

The resulting solid calcium carbonate was then separated through filtration. The recovered sodium hydroxide was returned to the air contactor, allowing continuous CO_2 capture. Meanwhile, the separated calcium carbonate was directed to a calciner, operating at ~900°C and 1 bar. In the calciner, $CaCO_3$ is thermally decomposed into calcium oxide (CaO) and pure gaseous CO_2, at the design flowrate of ~500 kmol/h. Finally, the calcium oxide from the calciner underwent slaking in a dedicated unit, maintained at approximately 300°C and atmospheric pressure. Here, CaO reacts with water to regenerate calcium hydroxide, which was then recirculated back to the pellet reactor, thus completing the closed-loop cycle of the DAC process [51]. The tabular stream results are presented in **Table S2** on Supplementary Document.

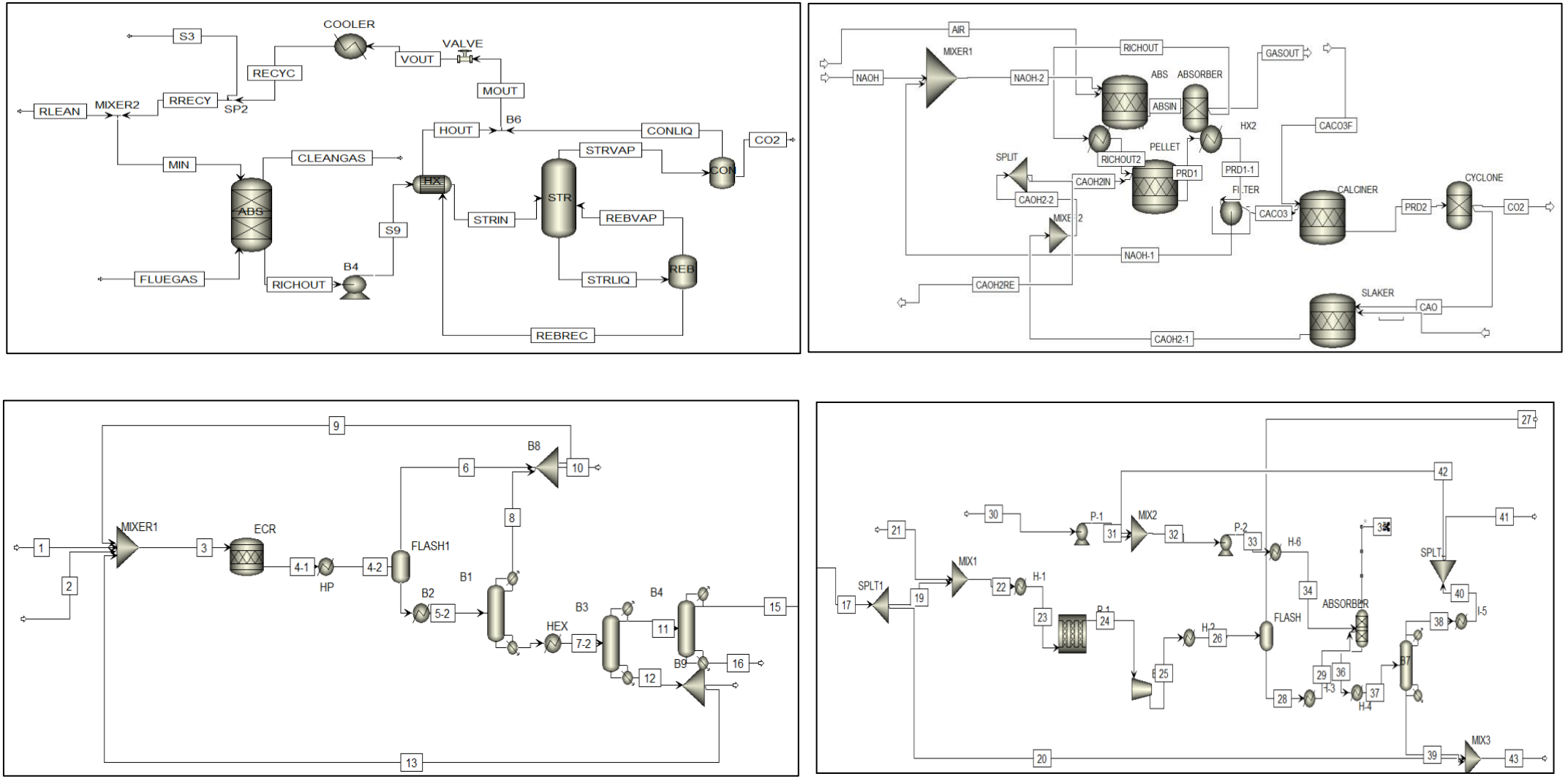

Figure 2: *Process Flow Diagrams for (a) PCC Process (b) DAC (c) Methanol Synthesis (d) Formaldehyde Production (from the top left to the bottom right)*

4. Economic Analysis

This section presents economic insight to the process, covering all investigated scenarios to identify key cost drivers and opportunities for improvement.

4.1. Base Case Cost Analysis

CAPEX and OPEX were used as primary metrics to evaluate the economic performance of each scenario (see **Table 4**). The fixed capital cost was calculated using total capital cost estimates from the Aspen Process Economic Analyser (APEA), with an additional 10% allocated for working capital [52]. The OPEX included costs related to labour, raw materials, utilities, maintenance materials, selling, general, and administrative (SG&A) expenses - each of which were essential for sustaining continuous operation. According to Turton, operating labour requirements were estimated using the following empirical correlation to first determine the number of operators required per shift (N_{OL}) [52]:

$$N_{OL} = \left(6.29 + 31.7P^2 + 0.23N_{np}\right)^{0.5} \quad \textbf{(E9)}$$

The terms P and N_{NP} resembled the number of particulate and non-particulate handling process steps, respectively. A rota factor of 4.5 was applied to the calculated N_{OL} to ensure adequate staffing for continuous plant operation and ethical labour conditions [52]. Assuming an average annual wage of $52,900 per operator, the total labour cost was determined accordingly [52]. Maintenance materials and SG&A costs were assumed as fixed percentages of the CAPEX, calculated as 5% and 10%, respectively [53]. Raw material costs were found on **Table 3**, referenced from suitable databases, and utility costs were directly obtained from APEA estimates. It was important to note that the electrocatalytic reactor (ECR) for methanol synthesis was modelled with a RStoic model in Aspen Plus. Therefore, in order to get reliable insights to CAPEX and utility contributions of the ECR, literature provided Equations **E10-E12**, which were used to calculate the CAPEX and utility costs of the reactor [54].

$$A = \frac{I_4}{J} \quad \textbf{(E10)}$$

$$CAPEX_{ECR} = A \times P_{electrode} \quad \textbf{(E11)}$$

$$C_{UT,ECR} = VI_4t \times P_{electricity} \quad \textbf{(E12)}$$

I_4 is current required by **R10**, A is surface area (cm^2) for electrodes, J is current density (A/cm^2), P defines the price, V is required voltage, and t is the operational time. The current density (0.3 A/cm^2), voltage (2V), and operational time (8000 hours) were sourced either from literature or Aspen Plus [54]. The RStoic equipment and utility costs estimated by Aspen Plus were removed and replaced by those calculated by **E11-E12** so that the total CAPEX and OPEX reflects the cost from electrocatalytic reactor appropriately.

Table 3: Raw Material costs

Material	*Cost*	*Unit*	*Location*	*Reference*
Deionised Water	0.001	$/kg	-	[52]
Air Pumping	0.0035	$/m^3	-	[52]
Fe catalyst	0.32	$/kg	Reactor (FA)	[55]
CO_2	0.214	$/kg	-	[56]
MEA	1.37	$/kg	PCC node	[57]
NaOH	0.23	$/kg	DAC node	[58]
$CaCO_3$	0.26	$/kg	DAC node	[59]

Table 4: Economic Evaluation of Base-case scenarios

Base Case Scenarios	*CAPEX ($)*	*OPEX ($/yr)*
No CO_2 capture	108,000,000	427,000,000
CO_2 sourced from PCC unit	120,000,000	395,000,000
CO_2 sourced from DAC unit	119,000,000	519,000,000

Across all three scenarios, CAPEX and OPEX were largely dominated by the ECR unit and utility costs - $86.5 million and $343 million/year, respectively. The ECR alone accounted for at least 68% of CAPEX and 66% of OPEX, signifying the challenges of electrocatalysis in large scale processes. Comparing CAPEX across scenarios, both PCC and DAC were more expensive than the 'No CO_2 Capture' case due to the additional process equipment required, though their total costs differed by only $1 million. When ECR utility costs were excluded, the main OPEX drivers shifted. For the 'No CO_2 Capture' scenario, purchasing CO_2 from Stora Enso's Langerbrugge site became the largest contributor, making up 10% of total OPEX. In DAC, the major cost was from $CaCO_3$, reaching $114 million/year (22% of OPEX), due to the large quantities needed to extract CO_2 from air at the required throughput. Since the variation in OPEX across scenarios was much more significant than that in CAPEX, OPEX became the deciding factor in selecting the best option. Based on this, PCC was identified as the most cost-effective scenario and is carried forward in the optimisation.

4.2. Downstream/Commercialisation

The final product was a mixture of manufactured formalin (for vaccine production) and sold MeOH (for commercialisation purposes). This ultimately depended on the product allocation ratio (PAR) – the proportion of MeOH directed towards formaldehyde production against the proportion sold commercially. To obtain this optimal ratio, a cost function was defined (**E13**), a simplified process representation was used. This simplified the analytical process by neglecting complex reaction kinetics, whilst providing the plant's segmented breakdown of time-series behaviour. The total MeOH produced, as determined from Aspen simulations, was fixed at approximately 62,000 tonnes per year. This MeOH could either be sold directly or used to produce formaldehyde. MeOH, traditionally priced at $0.64/kg, was elevated in its "e-MeOH" variant to $1451 per tonne, translating to approximately $1.45/kg with currency conversion (1 EUR = 1.1 USD) [60]. This premium reflected its green production route, using captured CO_2 and renewable hydrogen. The downstream impact of this pricing was evident in the formaldehyde market: while regular formalin sells at $0.37/kg, green formalin produced from e-methanol was calculated at $0.84/kg, a value derived from the relative pricing of e-MeOH to conventional MeOH, applied to formalin [61], [62]. This substantial premium offered strong revenue potential if market acceptance and policy incentives aligned with green product adoption.

Specifically, formaldehyde prices were adjusted in 5% increments over a range of ±30% around a base value of $0.84 /kg, creating a set of 13 scenarios. The model included a fixed conversion ratio of 1.5, meaning 1 kg of methanol yielded 1.5 kg of formaldehyde as taken from Aspen. A minimum of 10% of methanol was required to be fed in formaldehyde production, reflecting assumed internal demand or strategic constraint in addition to capital associated. Additionally, the cost of formaldehyde production was modelled as a function of the fraction of MeOH used, based on Aspen cost outputs (*see* **supplementary information**.)

The cost function (C) used was:

$$C = 734{,}394 \cdot y + 20{,}000{,}000 \quad \textbf{(E13)}$$

where y is the fraction of MeOH devoted to formaldehyde production and represents a linear approximation of the function. The objective was to maximise the net margin, defined by revenue from both sold MeOH and FA, minus the feed input costs as this did not impact the decision making for split fraction. **Table 5** provides model outcomes under multiple percentage scenarios of MeOH splits, reflecting different price levels and allocations. The sensitivity analysis revealed that at prices above $0.98 /kg of formalin (approximately 17% higher than current assumed price), converting all DOI MeOH to formalin is the most profitable strategy. If the formaldehyde price dips below $0.98 /kg, direct methanol sale becomes more competitive, although the ten-percent minimum usage constraint for internal formaldehyde demand still applies.

Table 5: Scenarios for price variations and split decisions

Price	*Change*	*Split Output*	*Net Margin ($)/year*
$0.59	0.70	0.1	7.32E+07
$0.63	0.75	0.1	7.36E+07
$0.67	0.80	0.1	7.40E+07
$0.71	0.85	0.1	7.44E+07
$0.76	0.90	0.1	7.49E+07
$0.80	0.95	0.1	7.53E+07
$0.84	1.00	0.1	7.57E+07
$0.88	1.05	0.1	7.61E+07
$0.92	1.10	0.1	7.65E+07
$0.97	1.15	0.1	7.70E+07
$1.01	1.2	1.0	8.07E+07
$1.05	1.25	1.0	8.47E+07
$1.09	1.30	1.0	8.87E+07

As shown in the supplementary material, net margin increased with higher formaldehyde output due to economies of scale, as increasing fraction offset the associated cost increases, lowering the production cost per kg at larger scales. Formalin, as a specialised product- particularly for vaccine-grade applications- is likely to command a greater price premium than the conservative e-methanol-based estimate which supports the full allocation of methanol to formaldehyde production, as partial production scenarios were found to be economically suboptimal, indicating an all-or-nothing outcome.

5. Optimisation

In this section, optimisation strategies are employed to improve process efficiency.

5.1. FORMOX Reactor Optimisation

The main optimisation method employed was a simple grid-search approach using sensitivity analysis within Aspen Plus. Due to no recycle stream around the reactor, this method allowed to find a solution without violating both mass and energy balances. However, the method still faced limitations concerning the pressure drop, thus pressure drop was neglected during grid-search. The objective function **(E14)** for the reactor optimisation was defined as follows:

$$\max\left[P_{FA}M_{FA} - \left(P_{cat}\frac{\rho_b V}{t} + P_{utility}|Q|\right)\right] \qquad \textbf{(E14)}$$

P represents the selling price or cost of materials, M is the mass flow rate, ρ_b denotes the catalyst bulk density, V is the reactor volume, t indicates the catalyst operational lifetime before replacement, and Q represents the reactor heat duty. Specifically, P_{FA} was assumed to be \$0.37 per kg of formaldehyde, P_{cat} was \$0.35 per kg of catalyst, and $P_{utility}$ was $\$\,1.6 \times 10^{-8}$ per Joule, consistent with Aspen Plus electricity cost assumptions [62], [63]. The catalyst lifetime, t, was assumed as 250 hours, according to literature [64]. Thus, the objective function defined represents the operational profit achievable from the reactor per second.

The optimisation objective, as defined by the objective function, was explicitly formulated to minimise the material and utility cost of the reactor. However, this objective also implicitly contributed to the reduction of both CAPEX and OPEX across the broader FORMOX process. A higher formaldehyde production rate enabled the downstream separation units to meet product specifications with smaller equipment and reduced energy requirements. Additionally, an increase in formaldehyde conversion led to a lower recycle stream flowrate. Therefore, while the objective function was not explicitly designed to minimise the overall cost of the FORMOX process, it did induce indirect cost benefits. Nonetheless, it was important to note that such a reactor optimisation does not guarantee the global cost minimum for the entire process.

During grid search, the reactor assumed 8500 tubes, with parameter boundaries and equidistance discretisation points defined in **Table 6**.

Table 6: Parameter boundaries & equidistance discretisation points

	LB	*UB*	*Points*
Diameter (m)	0.001	1.501	11
Length (m)	1	15	11
Temperature (℃)	250	400	11
Pressure (bar)	0.1	10.1	11

Even though each parameter dimension included only 11 equidistant points, the grid search explored a total of 14,641 data points. Given the relatively narrow parameter range, the number of data points was considered sufficient to cover the operational spectrum.

Temperature boundaries were chosen to balance catalyst performance, energy efficiency, and safety. While iron molybdate catalysts retained their morphology and selectivity up to ~600 °C [65], the upper limit was conservatively set at 400°C to mitigate thermal runaway risks and enhance reactor controllability. Conventional FORMOX reactors typically operate at atmospheric pressure and 250–400 °C to suppress side reactions [66], [67]. As we can see from the **Table 6**, the lower bound for the pressure is set at 0.1 bar, which arbitrarily defines the vacuum operation. This was in purpose to see the influence of pressure on the formaldehyde production. The top 2 optimal solutions identified from the grid search is summarised in **Table 7**.

Table 7: Top 2 optimal solutions from grid search

	Diameter (m)	*Length (m)*	*Temp (℃)*	*Pressure (bar)*	*Objective ($/sec)*
1	0.151	1	400	0.1	49.30
2	0.151	1	400	1.1	49.28

According to the grid search results, the best objective value was observed at near vacuum operation. Despite the short reactor length, which will cause very small pressure drop across the reactor, we have decided that the optimised reactor should be designed with pressure at 1 bar. This is due to the engineering decision with strong focus on process stability and safety. Albeit the small pressure drops, the real-life scenario cannot ensure perfect steady-state conditions. Hence, smaller inlet pressure will pose limited operability, thereby a very small flexibility index, of the reactor and the process. Moreover, additional operation cost for heat exchanger to ensure 0.1 bar might not be compensated with the infinitesimal increase of the objective value. Therefore, the optimised reactor will operate at 1 bar, 400℃, and dimension of 0.151m in diameter and 1 m in length.

As mentioned about the cost effect of reactor optimisation, according to the economic analyser of Aspen Plus, the reactor optimisation reduced the CAPEX and OPEX of FORMOX process from \$ 4.32M and \$ 3.19M to \$ 3.60M to \$ 2.49M, respectively. Therefore, the optimisation reduced the cost of FORMOX process by 16.7% and 22.1% respectively for CAPEX and OPEX. However, considering the cost of methanol synthesis process being extremely high, the impact of cost reduction on overall process might not be big enough.

One must note that because a grid-search optimisation method was employed, the solution identified represents a suboptimal solution. Nevertheless, this optimised solution demonstrates a better objective value compared to the base case reactor design, thus validating the effectiveness of the approach.

5.2. Post-Combustion Capture Optimisation

A sensitivity analysis was conducted on the PCC node in attempts of minimising the costs. Given that the majority of energy consumption occurs in the reboiler, the analysis focused primarily on the stripping section of the process. The heat exchanger (HX) design specification was also adjusted to (1) assess any dependencies between the HX design and other process equipment, and (2) explore the effect on the stripping performance, notably the CO_2 product flowrate. Therefore, this section will focus on temperature adjustments on both the rich amine stripper inlet stream temperature and the reboiler temperature.

5.2.1. *Heat exchanger sensitivity*

The rich amine stripper inlet stream was varied from 84-112 °C in increments of 4°C, which was compared to the base case of 110°C. The column sizing was also adjusted to maintain a consistent flooding capacity, with an error of ±3%. Temperature variations had little to no effect on the CO_2 product flow rate, with a range of 1.94 kmol/h. This minimal change in CO_2 flowrate suggested that the stripping column operation was relatively insensitive to moderate changes in rich amine inlet temperature. This was likely due to the reboiler compensating for thermal variations, maintaining the necessary conditions for CO_2 desorption. Despite the CO_2 flow remaining largely unaffected, variations in the cold outlet temperature had a significant impact on energy duties of the HX and cooler duty (COOLER), shown in **Figure 3**. As the rich amine temperature increased, heat exchanger duty increased steadily from 52,583 kW to 101,564 kW, reflecting the larger thermal lift required to preheat the stream. At the same time, the cooler duty upstream of the absorber decreased from 50,405 kW to 15,228 kW, since less heat needed to be removed from the lean amine exiting the stripper.

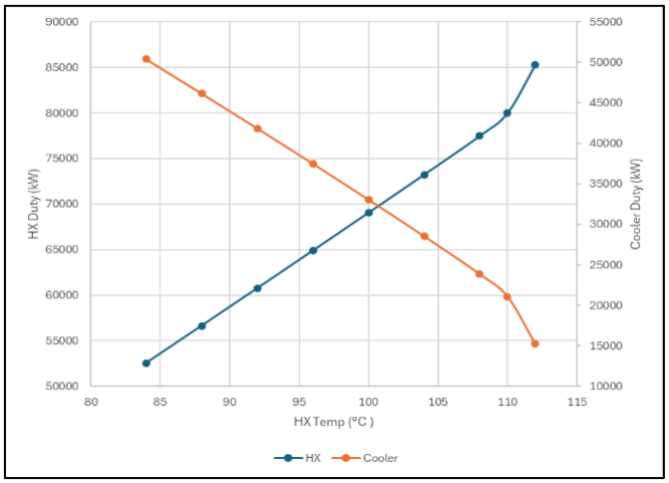

Figure 3 - Effect of HEX temperature specification on HEX and COOLER duties

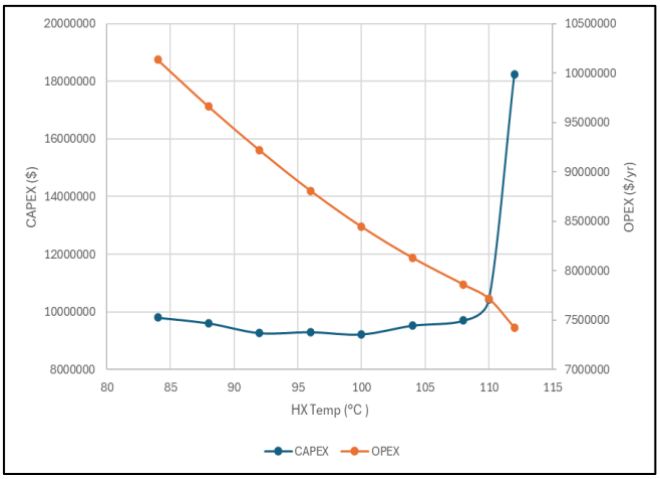

Figure 4 - Effect of HX temperature specification on PCC CAPEX and OPEX

These results demonstrate a clear energy trade-off: lower rich amine temperatures reduce the HX duty but increase cooler duty and vice versa. **Figure 4** illustrates the comparison between CAPEX and OPEX. In the range of 84-110°C, the CAPEX remained insensitive to temperature changes, with a sudden increase between 110-112°C. The OPEX variation was based solely on changes in cooler utility (assuming other changes are negligible) and saw a gradual decrease. The optimal point was therefore located at 110°C - the base case, with a CAPEX and OPEX of $10.4 million and $7.72 million/yr, respectively. A table with detailed sensitivity results, including column sizing adjustments and CO_2 product flow, can be found in the supplementary documentation.

5.2.2. *Reboiler Sensitivity*

The reboiler temperature was varied from 116-123°C in increments of 1°C. Whilst the modal HX temperature was the optimal value in the **Section 5.2.1** (110 °C), adjustments were made to compensate for reduced HX duty in some of the cases. In addition, adjustments to the column sizing for the reboiler sensitivity were made to ensure consistent flooding capacity (±3%).

Table 8 - Key results from Aspen Plus REB sensitivity

Reboiler Sensitivity	***Reboiler Temperature (°C)***							
	116	***117***	***118***	***119***	***120***	***121***	***122***	***123***
CO2 Product Flow (kmol/h)	445.5	456.2	468.0	482.3	500.5	525.54	555.5	558.3
HX Duty (MW)	56.98	58.91	80.39	82.89	79.99	79.51	73.29	56.79

Figure 5 illustrated the effect of reboiler temperature on the CAPEX and OPEX of the PCC process. An initial increase in CAPEX was observed, followed by a minimum at 120 °C, and a subsequent rise beyond this point. This trend correlated with the heat exchanger (HX) duty, which peaked at 119 °C (as shown in **Table 8**), reflecting the increased equipment and utility requirements for thermal integration. The secondary rise in CAPEX beyond 120 °C was attributed to a sharp increase in column sizing, driven by changes in vapour-liquid equilibrium and flooding constraints.

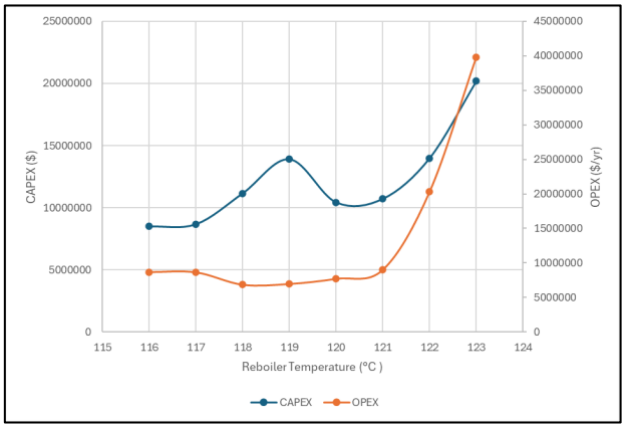

Figure 5 - Effect of Reboiler temperature specification on PCC CAPEX and OPEX

The OPEX trend showed an initial decline from 116–118 °C, due to reduced cooler duty requirements as HX duty increases – consistent with the discussion in the **Section 5.2.1**. However, beyond 120 °C, OPEX rose sharply, primarily due to a significant increase in medium-pressure steam (MPS) demand. This was reflected in a sudden jump from $9.04 million to $39.8 million per year between 121–123 °C.

Two local optima were identified: 117 °C and 120 °C. While CAPEX and OPEX were both favourable at 117 °C, the associated CO_2 product flowrate was only 456 kmol/h, compared to 500 kmol/h at 120 °C. Given that the downstream process required a minimum of 500 kmol/h, the data for 117 °C was scaled by 8% to meet this demand. The resulting adjusted CAPEX and OPEX were $11.6 million and $7.91 million/yr, both higher than those at 120 °C. Therefore, 120 °C was selected as the optimal reboiler temperature, offering the best balance between CAPEX, OPEX, and product specification - $10.4 million and $7.72 million per year respectively. This also confirmed the validity of the base case selection.

5.2.3. *Solvent Optimisation*

Whilst MEA could be conventional in an industrial setting: (1) It undergoes unwanted reversible reactions, reducing the amount of

active MEA content [68], [69].(2) MEA often degrades into unwanted products through thermal and oxidative degradation to form Formic/Acetic/Oxalic/Glycolic acid and/or irreversible salts. At temperatures above 120℃, MEA could undergo thermal degradation and form OZD, a highly stable carbamate intermediate, which was difficult be convert back to MEA [70]. (3) MEA introduces volatile amines to be released to the top of the absorber, whilst simultaneously accumulating organic acids at the bottom. Further emission of amines could undergo photo-oxidation/degradation into Nitrosamines or Nitramines, which are mutagenic and carcinogenic [68].

Through this discussion, an alternative had been considered to improve process performance. An optimisation problem using CAMD (Computer Aided Molecular Design) could help, by iteratively combining different molecular functional groups to form unique molecule structures, where each functional group will contain unique individual properties [71]. This used a group contribution method, which estimated the properties/values of the hypothetical solvent structure when functional groups are combined. The properties looked to determine from literature are T_b , T_m , V_m , Relative Energy Difference (RED), and c_p; which could be done using the following. (1) A property prediction method proposed by Hukkerikar using the MG (Marrero and Gani) group contribution method, to estimate T_b, T_m, V_m properties of pure components [71]. (2) A study by Adjiman et al. to determine the relative energy density (RED), as supported by B. Kjærside Storm [72], [73](3) A report by Henni et al. to estimate C_p based off a group additivity analysis (GAA) [74].

The following additional constraints were added in order to restrict the solvent's structure: (1) T_m to be less than the average temperature of the absorption column (299K) to avoid solvent solidification. (2) T_b to be higher than the average temperature of the desorption column (388K) to avoid excess vaporisation of the pure solvent. (3) Presence of the octet rule to ensure zero molecular valency and no free bonds [75]. (4) Presence of the bonding rule to prevent undesired combinations of the molecule [76]. This ended up posing an MINLP optimisation problem. The overall objective function was posed such that RED < 1, C_p is minimised, ρ_l is maximised, all of which presented using a weighted-sum method, ensuring consistent magnitude within all terms [72]. Respectively, this ensured that solvent regeneration was reduced as it accounted for 60-80% of energy consumption, heat of absorption for solvent regeneration was reduced, and solvent density was maximised to reduce pumping requirements [76], [77]

$$\max \rho$$

$$\min RED, C_p$$

$$\text{s.t. } T_m < 299\text{K}$$

$$T_b < 388\text{K}$$

$$RED \leq 1$$

The problem utilised the following set of equations for the CAMD problem, where OP and AP refered to objective and additional properties respectively.

1. Objective Function Definition

$$\min Z(RED, C_p, \rho_l)$$

$$Z = \sum_1^{n_{OP}} w_{OP_i} * \frac{OP_i - OP_{i_{max}}}{OP_{i_{min}} - OP_{i_{max}}}$$

$$\text{s.t. } 0 \leq OP \leq 1000 \text{ , } OP \in \{RED, C_p, \rho_l\}$$

$$-10000 \leq AP \leq 10000 \text{ , } AP = \{T_m, T_b, \delta_D, \delta_H, \delta_P, V_m\}$$

2. Design Space/Functional Group Selection

$$G = \{\text{design space}\}, 0 \leq n_G \leq 15, 0 \leq \sum_{k \in G} n_k \leq 15$$

$$0 \leq n_{40} \leq 2 \text{ , } 0 \leq n_{44} \leq 2$$

$$-1 \leq m \leq 1$$

3. Octet and Bonding Rule/Feasibility Constraints

$$\sum_{k \in G} n_k (2 - v_k) - 2m = 0$$

$$n_k(v_k - 1) + 2 - \sum_{q \in G} n_q \leq 0 \text{ , } \forall k \in G$$

$$393 - T_b \leq 0 \text{ , } T_m - 313 \leq 0$$

$$y_a + y_m + y_b = 1$$

$$m - (y_a - y_b) = 0$$

4. Cyclic Structure Constraint

$$CG = \{\text{cyclic group}\} \; ACG = \{\text{Acyclic Group}\}$$

$$\sum_{c \in CG} n_c = 6y_m + 10y_b$$

5. Literature Equality Constraints

$$RED = \frac{R_a}{R_0}$$

$$R_a^2 = 4\left(\delta_{D,CO_2} - P_{\delta_D}\right)^2 + \left(\delta_{P,CO_2} - P_{\delta_P}\right)^2 + \left(\delta_{H,CO_2} - P_{\delta_H}\right)^2$$

$$\rho = \frac{1}{V_m}$$

$$f(X) = \sum_{a \in ACG} n_a \phi_a + (1 - y_a) \sum_{c \in CG} n_c \phi_c$$

$$f(T_m) = \exp\left(\frac{T_m}{T_{m0}}\right)$$

$$f(T_b) = \exp\left(\frac{T_b}{T_{b0}}\right)$$

$$f(V_m) = \exp\left(\frac{V_m}{V_{m0}}\right)$$

Using the weighted-sum method, four unique cases (as shown on **Table 9**) were analysed. **Case 1 - 3**: Majority of emphasis was placed on satisfying property OP. **Case 4**: All properties had equal emphasis. To ensure previous combinations were not generated again, integer cut had been implemented. This reduced the feasibility region, making a mixed integer problem more suitable to solve [78].

Table 9: Experimented Cases

Case	*RED*	C_p	ρ_l
1	0.50	0.25	0.25
2	0.25	0.50	0.25
3	0.25	0.25	0.50
4	0.33	0.33	0.33

To form our theoretical solvent structure, all possible functional groups must be specified. **Table S6** in the supplementary document indicated the enumerated design space with a unique number ID to identify each group individually. These were selectively chosen based off manual assessment. The GAMS optimisation exhibited the following solvent structures, alongside the following properties.

Table 10: Final Solvent Structure Properties

Case	T_m	T_b	*RED*	ρ_l	c_p	*OF*	*Solvent Functional Groups*
1	267.6	453.8	0.0445	6.0350	400.41	0.0003	3x CH3, 1x CH, 1x C, 2x CH2NH
2	242.1	427.1	0.4971	9.6154	200.50	0.0231	1x CH3, 1x CH3CO, 1x CH2O, 1x -O-

3	274.2	424.2	1.041	7.7280	272.12	0.1964	2x CH3,1x CH2,1x CH2CO, 1x CH2NH
4	215.6	407.1	0.432	9.302	195.3	0.0589	2x CH3,1x CH2, 1x -O-,1x >CO

Based off the following analysis, Case 1 had provided the optimal solvent properties with the lowest objective function. This represented the common structure of N-isopropylethanamine, a secondary amine as shown in **Figure 6**. This structure followed close to preferential properties of CO_2 absorbers due to the following: (1) Presence of N atoms facilitating nucleophilic interactions with CO_2 [79] (2) No presence of cyclic structures, as cyclic structures were generally less soluble, more volatile, and undergo steric hindrance which could reduce their effectiveness [80] (3) No amine or hydroxyl groups within close proximity, maintaining basicity and ensuring carbamate formation [81] (4) No indication of double/triple bonds which minimises generation of by-products, maintaining the solvents longevity at high temperatures [82].

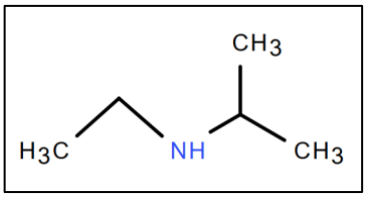

Figure 6: N-isopropylethamine structure (Based of Solvent Optimisation)

5.2.4. Heat Integration

Heat integration was conducted using Aspen Energy Analyser V14. The detailed Heat Exchanger Network (HEN) was presented on supplementary document (**Figure S3**). The largest and most significant heat exchanger in the dataset was labelled E-129, which handled a massive heat load of approximately 52 million kJ/h. This exchanger had the highest associated cost, exceeding $841,000, indicating that it was both a technically and economically dominant component in the integration scheme. With a heat transfer area of over 3500 square metres and eight shell passes, E-129 was clearly designed for heavy-duty service, possibly involved in condensing large process vapours or interfacing with major utility systems like air coolers or condensers. The log mean temperature difference (LMTD) for this unit was moderate at around 39.8°C, and the overall heat transfer coefficient was about 383 kJ/h·m²·°C, a reasonable value given the large surface area and moderate driving force.

In contrast, other exchangers such as E-114 and E-116 handled significantly smaller loads of around 5.4 million kJ/h and 10 million kJ/h, respectively. E-114 exhibited a very high LMTD of over 170°C but a low overall heat transfer coefficient of only 68.1 kJ/h·m²·°C, which suggested that either the heat transfer process was limited by the fluid properties or that it was using a less conductive material or a fouling-prone stream. Its cost was much lower than E-129, at around $125,000, with a relatively small area of 500 square metres and just one shell pass. E-116, by comparison, had a strikingly high overall heat transfer coefficient, over 1800 kJ/h·m²·°C, despite a smaller area and LMTD. This high value indicated a highly efficient exchange, likely between two clean and compatible process streams, which supported effective integration.

Another noteworthy exchanger was E-134, which operated in a cryogenic zone of the process. It cooled a hot stream from -21°C down to -66°C, and in doing so interfaces with Refrigerant 4, which entered the system at -103°C and exited at -102°C. This marginal increase in refrigerant temperature signified its role as a heat sink, accepting just enough thermal energy to maintain low operating temperatures in this unit. The heat load here was significantly smaller, at just under 3 million kJ/h, and the equipment cost is about $38,000. This exchanger was likely serving a key role in the methanol or formaldehyde purification or recovery section, where sub-ambient processing was often essential.

From a thermal integration standpoint, the dT_{min} values for hot and cold streams gave clues about how close each exchanger operated to its pinch point. For example, E-114 had extremely high temperature differences, $dT_{min\ (HOT)}$ of 225.9°C and $dT_{min\ (COLD)}$ of 125.2°C, which meant the streams were far from pinch and could exchange heat very easily, reducing the need for additional surface area. In contrast, E-132 operated with much tighter margins, especially on the cold side, where $dT_{min\ (COLD)}$ was less than 4°C. This small difference implied that the exchanger was operating close to the thermodynamic limit, likely requiring precise control and potentially contributing to the energy bottleneck in the system. Overall, this dataset showed a clear picture of a well-integrated chemical plant with strategically selected heat exchangers, each serving specific thermal roles, ranging from large-scale condensation and recovery (E-129), medium-scale energy shifts (E-114, E-116), to fine-tuned cryogenic operations (E-134). The combination of performance metrics such as LMTD, heat transfer coefficient, and area, along with economic indicators like cost index, reflected the engineering trade-offs between efficiency, feasibility, and capital investment.

6. Feasibility Studies

The economic model assumed that the project would be fully equity-financed, meaning no capital loan and consequently, no burden from interest payments. This simplified the Net Present Value (NPV) analysis with inflation of 3% and focused the evaluation on operational profitability and capital efficiency. Catalyst replacement was assumed on a six-month cycle, adding a recurring operational cost. Inflation was imposed at 3% annually, influencing long-term cost and purchasing power assessments, although the presented NPV table used a 0% discount rate, isolating the real cash flow performance without the impact of temporal value adjustments [66].

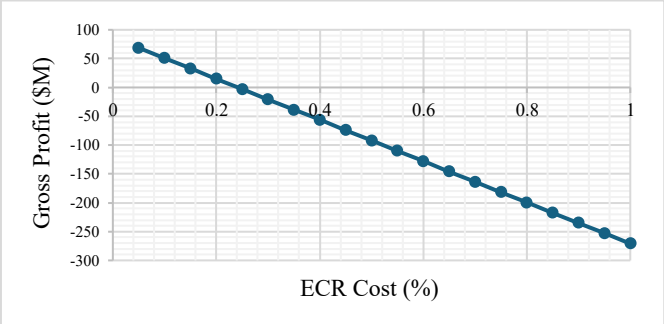

Figure 7: Gross Profit Sensitivity Analysis ($M) vs ECR Cost (%)

A unique aspect of this analysis was the treatment of ECR-related costs, likely tied to environmental compliance or carbon reduction technologies. Consequently, the sensitivity analysis for gross profit ($M) vs. ECR Cost (%) was conducted assuming gross profit equals to revenue minus operating costs and shown in **Figure 7**. From the results, instead of assuming traditional cost burdens, it was noted that ECR costs were only 20% of the actual costs. This suggested an optimistic outlook, potentially due to technological advancements or government subsidies reducing the financial impact of green compliance. Product pricing played a central role in revenue estimation as discussed previously in **Section 4.2**.

The NPV analysis indicated a heavy initial investment, reaching a total cost of $11.64M in year 0 and $178.79M by year 20 due to inflation. Following the plant startup schedule on **Table 11**, revenue began modestly in year 3 at $36.32M and scaled up to over $200M annually by year 20. From year 4 onwards, the project generated consistent gross profits of $17–27M annually, with a tax rate of 25% applied to taxable income after accounting for a fixed depreciation of $1.94M per year, which was derived from fixed capital cost over 20 years of plant operation [83]. Taxes gradually rose along with profits, starting at $2.91M in year 3 and reaching $6.33M by year 20.

Finally, the total NPV turned positive around year 6–7, crossing from a cumulative loss of $-10.65M at year 5 to a gain of $3.18M at year 6,

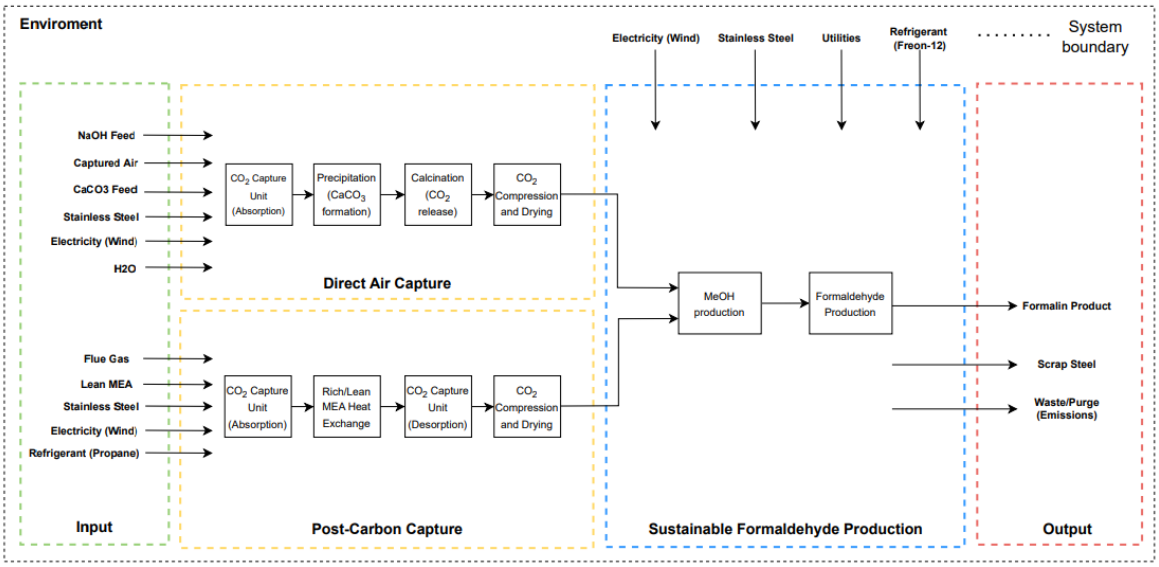

Figure 8: Cradle-to-Gate Diagram

eventually rising to a cumulative value of $245.43M by year 20. The detailed results were written on **Table S5** on Supplementary Document. Crucially, this indicated the payback period is 6 years, whereby the end of year 6, the cumulative cash inflows exceeded the total capital outflows. This opened a relatively robust investment opportunity, given the low risk from financial leverage and the premium pricing potential in green chemicals. Both figures demonstrated that both long-term viability and resilience against uncertainties in early capital deployment, assuming sustained demand for green formaldehyde.

Table 11: Typical Chemical Plant Startup Cost-related Schedule)

Year	***Cost***	***Revenue***
1st year	30% of fixed capital	-
2nd year	60% of fixed capital	-
3rd year	10% of fixed capital + Working capital + FCOP + 30% of VCOP	30% of revenue
4th year	FCOP + 90% VCOP	90% of revenue
5th year +	FCOP + VCOP	100% of revenue

7. Environmental Analysis

7.1. Introduction to LCA

To quantify the environmental impacts of the process, a life cycle assessment was performed. This compared the impacts of all possible scenarios identified environmental hotspots and provided recommendations for improvement of the cradle-to-gate process. A functional unit (FU) of "one unit of formalin production (kg) from an industrial facility in a 20-year lifespan operation" was selected, to ensure fair comparability across all relevant scenarios. The assessment was based off the ASPEN Plus Simulation data, along with several assumptions such as the sourcing of auxiliary feedstock materials. Utility usage was selectively chosen from the ASPEN Energy Analyser, with a mixture of Freon-12 refrigerant, steam in chemical industry, cooling water, and electricity (supplied by wind), all of which were relatively environmentally friendly. A 'chemical factory' constant of **4E-10** was assumed for all processes, to account for the material and construction efforts of refinery infrastructure, originally derived from the construction of a distillation unit, in which according to OpenLCA simulation descriptions, the European Commission stated that the distillation unit was the most frequently used unit operation within the production of all major organic chemicals to estimate the composition of the overall unit operation infrastructure. For consistency, a continuous operation time of 8000 hours a year was also assumed. The simulation also accounts for crediting CO2 capture where necessary.

The life cycle impact assessment (LCIA) method "ReCiPe Midpoint (H) V1.13" was utilised to assess 18 possible impact categories. Using a hierarchist approach, similar to a default scientific model, this allowed us to implement a broad set of mechanisms, where sufficient global insight was provided [84]. **Figure S4** (*see* Supplementary Document) summarises the relevant impact categories with the largest contributors to environmental burdens, fossil depletion, GWP, human toxicity, to all possible cases. To illustrate, **Figure 8** represents a Cradle-to-Gate diagram of all possible routes.

7.2. Global Warming Potential Discussion

Analysing the base case alone, the GWP-100 exhibited was 3.90 $kgCO_{2eq}$. For reference, a study by Leila et al. mentions that the GWP of a conventional unit formalin production process was around 386.3 $kgCO_{2eq}$ [85]. Leila mentioned how evident it is that most of the life cycle contributions for formalin production is expelled from the production of MeOH and consumption of non-renewable/fossil fuel resources which aligns closely to the deductions [85]. Furthermore, Leila's life cycle inventory data assumed that 0.29g would be sufficient for the functional unit of 1 ton of formalin, which lacked reproducibility to validate the OpenLCA results obtained, possibly due to ulterior assumptions [85]. Another study by Myat has indicated that producing 1000 kg of formalin in Thailand exhibited a GWP of 3077 $kgCO_{2eq}$, with efficiently utilised CO_2 [86]. Assuming linear scale down to 3.07 $kgCO_{2eq}$ for 1kg of formalin production, this was an indication that our process could be optimised further for reduced carbon efficiency. However, Myat presented a strong argument stating that various products and co-products could be discounted from the final GWP as they are not intentionally produced as part of the primary products lifecycle but are instead repurposed for alternative means [86]. For example, with the intention of selling MeOH at an earlier stage, this could have been discounted from the final GWP and instead sold commercially rather than processing further. By neglecting 'sold' MeOH out of the scope of GWP, a more realistic impact assessment can be presented.

The same assessment was performed for the optimised base case formalin process, where the GWP was 4.05 $kgCO_{2eq}$. This was strongly as a result of the MeOH outlet flowrate in the main product stream being around 2.5 times larger. The optimised configuration could have been further improvised, as un-intended MeOH produced could be recycled in order to reduce the overall GWP. An additional consideration to reduce atmospheric CO_2 concentration was to pair the optimised formalin process with DAC and PCC. Surprisingly, the GWP-100 of CO_2 captured cases surpassed those without. All processes (base case and optimised) which used DAC were amongst the highest GWP-100 (22.3 and 23.1 $kgCO_2$-eq respectively) producers, largely due to calcium looping cycle in the DAC process. The presence of $CaCO_3$ encouraged quicklime (CaO) production along with CO_2 as a by-product, which was modelled as process emissions into the environment. Electricity production via lignite minerals, a

non- specified direct input in OpenLCA, also stemmed a high GWP-100 value, drawing from the production of e-Chlor-alkali (NaOH) [87]. Lignite-based electricity (brown coal), accounted for 9% of EU's electricity production in 2020, with a lower carbon content than other fossil fuel-based electricity but still categorised as a non-renewable, which explains the following trend [88]. Both the base-case and optimised configuration of PCC, with optimised FA, both showed a GWP-100 of 4.05 $kgCO_2$-eq, with MEA solvent production accounting for 50.0 % of both PCC processes. Unsurprisingly, there was little to no difference between the two cases, as a result of the minimal impact of the sensitivity analysis via the reboiler attached to the stripper, as shown in **Section 5.21 and 5.2.2**. **Section 5.2.3** addresses an alternative solution through solvent development. Further studies are suggested to explore lower-impact options as this observation of CO2 capture technology cases having little to no improvement through optimisation was consistent across all situations.

7.3. Fossil Depletion Discussion (FDP)

To encourage consumption of renewables, the process had opted for electricity derived from wind energy only. However, in reality, to fill gaps in the energy demand, fossil-fuels must be exploited, as renewables exhibit intermittency and energy variability. This uplifts the depletion of non-renewable resources in all three optimised processes. The optimised FA process without had a FDP of 5.3E-04 kg oil-Eq, which can be considered insignificant. On the other hand, the optimised FA with base- and optimised-case PCC process also exhibited a FDP of 5.3E-04 kg oil-Eq, which was as expected as the carbon capture process did not introduce any fossil fuel consumption and/or consume energy from the same source. Finally, 99.99% (5.31 kg oil-Eq) of fossil depletion in the optimised FA with DAC was associated with the DAC process alone, where roughly equal contributions from air separation of O_2 and N_2, and $CaCO_3$ sourcing was present. Regardless, the relative magnitude of the DAC case was unsurprising, considering the amount of CO2 generated from the calcination reaction. In general, CCS processes are also known to exhibit intensive fossil depletion rates. Styring et al. mentions that 97% of fossil depletion in an MEA-based solvent CCS process was attributed to solvent regeneration, making it the most impactful factor relative to electricity and water consumption [89]. This statement can be justified, considering the contribution of water consumption and electricity consumption for air separation accounted for around 75% (4.2E-04 kg oil-Eq). Exploiting Belgium's alternative renewable-electricity sources such as Solar-PV would be suggested, as they account for 9.9% of total electricity production as of 2023, indicating abundance in supply [33].

7.4. Metal Depletion Discussion (MDP)

To mitigate abiotic depletion, the process must employ metallic elements/resources efficiently as such materials are expensive to extract, purify, and convert to a useful form. As for the optimised formaldehyde scenario without carbon capture, the former exhibited a MDP of 1.4E-04 kg Fe-Eq, predominantly from H2O sourcing and refrigerant requirements. Similarly to FDP, both cases of PCC integration exhibited the exact same FDP of 1.4E-04 kg Fe-Eq, indicating how PCC has no impact on metal depletion. As for the optimised formaldehyde case with DAC, $CaCO_3$ sourcing accounted for 58.47% of the total MDP of 0.68 kg Fe-Eq, largely linked to the chemical factory, consuming scarce resources such as Cadmium, electronics, and steel. Whilst this is a topic narrowly discussed in this sector; further research ought to be conducted for novel methods of MDP reduction, to preserve finite materials.

7.5. Energy Intermittency

To mitigate renewable's intermittency and variability challenges, Belgium has initiated the pursuit of constructing energy storage systems for battery use. Notably, Reuters mentioned how Sweco intend to design Europe's largest battery energy storage system by 2028, called Green Turtle [90]. This would stem a big step forward to reducing Belgium's dependence on gas powered plants as currently, the country relies on its abundance in wind and solar-PV renewable supply. To understand why, an additional sensitivity analysis was performed on OpenLCA simulation to determine the impact on different ratios of both energy sources. The simulation will assume wind and solar-PV energy as primary electricity sources, whilst biofuels are contingency purposes. Electricity consumption was allocated equally to wind and solar-PV whilst biofuels accumulated for the remainder total electricity supply that was not occupied, differing by 0.05 at each interval. For a detailed breakdown, see the energy allocation is described on **Table S6** (*see* Supplementary Document).

The simulation indicated consistent results regardless of the energy distribution, with the same GWP-100 of 4.05 $kgCO_{2eq}$. This was relatively surprising to witness and could possibly be the result of internal assumptions/model design choices made in OpenLCA, where most renewables often being considered as carbon-neutral in OpenLCA, indicating any CO_2 released has been offset by CO_2 absorbed into the process or the impact on GWP being negligible relative to other impact factors. The influence on agricultural land occupation for biofuels could be larger than GWP, as derived from biomass, often obtained through agriculture land. Overall, this is an indication that a renewable-only future is not the reality.

8. Conclusion

As part of Belgium's efforts to utilise captured CO_2, the following report evaluated three configurations for sustainable formaldehyde production: a base case without carbon capture, a post-combustion capture (PCC) route using MEA, and a direct air capture (DAC) pathway using NaOH. Whilst PCC and DAC demonstrated strong potential for emissions reduction and economic viability, the non-optimised base case alone still yielded the lowest GWP-100 of all configurations, at 3.90 kg CO_2-eq per unit product. Economic analyses further revealed that optimising the base case benefited from significant reductions in capital and operating costs, without the added complexity of capture systems. In contrast, the DAC route remained the most environmentally ambitious but economically prohibitive. Based on overall combined environmental and economic performance, the optimised PCC configuration emerged as the most sustainable and pragmatic solution for industrial-scale formaldehyde production in the near term. As an extension of the current research presented, energy intermittency can be touched upon further, as a more realistic scenario would employ a mixture of non-renewables alongside, such as nuclear fuels, natural gas, and coal-based resources, accounting for 40%, 21%, and 2% of Belgium's electricity mix respectively [33]. While the use of 14 wt% MEA does not reflect the industry standard of 30 wt%, the higher regeneration energy of 30 wt% MEA is often offset by its greater CO_2 absorption capacity. This leads to lower solvent circulation rates and potentially smaller equipment sizes [28]. Future studies can explore the impact of varying MEA concentrations on process performance. Furthermore, as no formal research has been performed (on the public domain) on N-isopropylethanamine as a CO_2 solvent, this is also a topic of further discussion as it was indicative of optimal solvent properties based off empirical formulation. With the three adopted approaches present, the report indicates that Belgium presents itself as a leading contender in utilising CO_2 optimised technology in domestic decarbonisation. Finally, when forecasting the price of e-MeOH, there exists major uncertainty. Forecasting a key-chemical's price can be seen as challenging, due to unprecedented black swan events and innovations over the next 20 years. From an outward looking perspective, the expectation of sustainable chemical production to be more in line with up-and-coming mandates and regulations is high. This may see a change in the market dynamic where more interest may be driven towards sustainable formalin production, making the following study more prevalent. Hence, given sufficient data, a more in-depth analysis would assist in giving a more comprehensive understanding on the cost-of production of sustainable formalin (and its intermediate counterparts).

9. Acknowledgements

Imperial College London's EURECHA representatives would like to extend our gratitude to the following members of staff: Dr. Maria Papathanasiou, Dr. Andrea Bernardi, all contributing members from the Papathanasiou Lab, and Professor Ronny Pini. This project would not be possible without their unwavering support and guidance.

10. References

[1] CCPI. (March). *CCPI (Climate Change Performance Index) - Belgium*. DOI: https://ccpi.org/country/bel/.

[2] BIEA. Belgium's greenhouse gas inventory (1990-2022) - national inventory document. Belgian Interregional Environmental Agency. Belgian Interregional Environmental Agency. 2024. DOI: https://climat.be/doc/nir-2024.pdf.

[3] The Brussels Times with Belga, "Healthcare sector generates 5% of Belgium's CO2 emissions," 2025. DOI: https://www.brusselstimes.com/1459753/healthcare-sector-generates-5-of-belgiums-co2-emissions.

[4] Jenna Philpott, "Pharma's path to Net Zero: Targeting Scope 3 emissions," 2023. DOI: https://www.pharmaceutical-technology.com/features/pharmas-path-to-net-zero-targeting-scope-3-emissions/.

[5] Carbon Credit Capital. *Net Zero Leaders in the Pharmaceutical Industry*. DOI: https://carboncreditcapital.com/net-zero-leaders_pharma/.

[6] R. Allen. (Jan 16). *Renewables accounted for nearly 30% of Belgium's power generation in 2024*. DOI: https://www.enerdata.net/publications/daily-energy-news/renewables-accounted-nearly-30-belgiums-power-generation-2024.html.

[7] Anonymous "Renewables near 30% of Belgian Power Mix," *Energy Monitor Worldwide,* 2025. DOI: https://www.proquest.com/docview/3151393969.

[8] Anonymous "Commission approves €682m Belgian State aid scheme to support renewable offshore wind energy," *Gulf Oil & Gas,* 2024. DOI: https://www.proquest.com/docview/3106781364.

[9] H. R. Gerberich and G. C. Seaman, *Formaldehyde.* 2004. DOI: 10.1002/0471238961.0615181307051802.a01.pub2.

[10] HSE, *Vaccine Ingredients*, 2022. DOI: https://www.hse.ie/eng/health/immunisation/hcpinfo/vaccineingredients/

[11] WHO, *WHO Expert Committee on Biological Standardization : Sixtieth Report.* 2013. DOI: https://pubmed.ncbi.nlm.nih.gov/24669583/

[12] USFDA. *Policy for testing of alcohol (ethanol) and isopropyl alcohol for methanol, including during the public health emergency (COVID-19); guidance for industry.* Federal Information & News Dispatch, LLC. Washington. 2021. DOI: https://www.proquest.com/docview/2492289291.

[13] L. Möller *et al*, "Evaluation of Virus Inactivation by Formaldehyde to Enhance Biosafety of Diagnostic Electron Microscopy," *Viruses,* vol. 7, *(2),* pp. 666–679, 2015. DOI: 10.3390/v7020666.

[14] The Business Research Company. (Jan). *Formaldehyde Global Market Report 2025*. DOI: https://www.thebusinessresearchcompany.com/report/formaldehyde-global-market-report.

[15] European Commission. *Task Force for Industrial Scale-up of COVID-19 vaccines*. DOI: https://single-market-economy.ec.europa.eu/coronavirus-response/task-force-industrial-scale-covid-19-vaccines_en.

[16] European Commission, "EU Vaccines Strategy," 2020. DOI: https://commission.europa.eu/strategy-and-policy/coronavirus-response/public-health/eu-vaccines-strategy_en.

[17] C. P. Bown and T. J. Bollyky, "How COVID-19 vaccine supply chains emerged in the midst of a pandemic," *World Economy,* vol. 45, *(2),* pp. 468, 2021. DOI: 10.1111/twec.13183.

[18] J. Puhar *et al*, "Review and environmental footprint assessment of various formalin production pathways," *Journal of Cleaner Production,* vol. 377, 2022. DOI: 10.1016/j.jclepro.2022.134537.

[19] I. Dincer. *Steam methane reforming*. 2018. DOI: https://www.sciencedirect.com/topics/engineering/methane-steam-reforming. DOI: https://doi.org/10.1016/B978-0-12-809597-3.00326-6.

[20] A. González-Garay *et al*, "Plant-to-planet analysis of CO2-based methanol processes," *Energy Environ. Sci.,* vol. 12, *(12),* pp. 3425, 2019, DOI: 10.1039/c9ee01673b.

[21] M. Qian, M. A. Liauw and G. Emig, "Formaldehyde synthesis from methanol over silver catalysts," 2002. DOI: https://doi.org/10.1016/S0926-860X(02)00340-X

[22] C. Fogler. (Jan). *Hydrogen: Future of Clean Energy or a False Solution.* DOI: https://www.sierraclub.org/articles/2022/01/hydrogen-future-clean-energy-or-false-solution#:~:text=Hydrogen%20can%20also%20be%20combusted%2C%20like%20gas%2Cto,and%20nitrogen%20oxide%20(NOx)%2C%20a%20harmful%20pollutant.&text=The%20production%20of%20hydrogen%20through%20steam%20methane,carbon%20monoxide%2C%20and%20volatile%20organic%20compounds%20(VOCs).

[23] Edward Zhang. *Comparing the Different Formaldehyde Production Processes*. 2025. DOI: https://www.phxequip.com/resource-detail/40/comparing-the-different-formaldehyde-production-processes

[24] A. Malandria *et al*, "Data-Driven Optimisation of Intermittent Methanol Production via Electrocatalytic Reduction of CO2 from Direct Air Capture," 2023. DOI: https://scholar.google.co.za/citations?view_op=view_citation&hl=zh-CN&user=CfxSo7IAAAAJ&citation_for_view=CfxSo7IAAAAJ:9yKSN-GCB0IC.

[25] J. Thrane *et al*, "A Review and Experimental Revisit of Alternative Catalysts for Selective Oxidation of Methanol to Formaldehyde," *Catalysts,* vol. 11, *(11),* pp. 1329, 2021. DOI: 10.3390/catal11111329.

[26] Stora Enso, "Stora Enso Langerbrugge paper site today - A center of circular excellence," *ENP Newswire,* 2024. DOI: https://www.storaenso.com/en/newsroom/news/2024/5/langerbrugge-paper-site-today.

[27] Endrava, "CaptureMap," 2022. DOI: https://www.capturemap.no/.

[28] C. Madeddu, M. Errico and R. Baratti, "SPRINGER BRIEFS IN ENERGY," 2019. DOI: https://link.springer.com/content/pdf/10.1007/978-3-030-04579-1.pdf

[29] Fern, "Belgium's largest biomass plant closes… for good," 2023. DOI: https://www.fern.org/publications-insight/belgiums-largest-biomass-plant-closes-for-good-2694.

[30] M. Mostafa *et al*, "Capturing CO2 from the atmosphere: Design and analysis of a large-scale DAC facility," *Carbon Capture Science &Amp; Technology,* vol. 4, 2022. DOI: 10.1016/j.ccst.2022.100060.

[31] Vynova. *Vynova - Caustic Soda*. 2019. DOI: https://www.vynova-group.com/products/caustic-soda.

[32] Veolia. *Rapide Strata™*. 2025. DOI: https://www.veoliawatertechnologies.com/en/solutions/technologies/rapide-strata.

[33] IEA, "Belgium," 2024. DOI: https://www.iea.org/countries/belgium.

[34] S. Hardman, "Managing the renewable energy intermittency challenge," 2024. DOI: https://www.powerengineeringint.com/feature-articles/managing-the-renewable-energy-intermittency-challenge/.

[35] Simões, H. M. & Erbach, G. Roadmap to EU climate neutrality - Scrutiny of Member States: Belgium's climate action strategy.2024. DOI: https://www.europarl.europa.eu/RegData/etudes/BRIE/2024/767175/EPRS_BRI(2024)767175_EN.pdf

[36] P. Adesina, J. W. Ager and A. A. Lapkin. P. Adesina, J. W. Ager and A. A. Lapkin. Beyond butler-volmer equation for CO2 electro-reduction on cu-based gas diffusion electrodes. American Chemical Society (ACS). 2024. DOI: 10.26434/chemrxiv-2024-hx5gr.

[37] J. A. Herron and C. T. Maravelias, "Assessment of Solar-to-Fuels Strategies: Photocatalysis and Electrocatalytic Reduction," *Energy Tech,* vol. 4, *(11),* pp. 1369, 2016. DOI: 10.1002/ente.201600163.

[38] M. Jouny, W. Luc and F. Jiao, "General Techno-Economic Analysis of CO2 Electrolysis Systems," *Ind. Eng. Chem. Res.,* vol. 57, *(6),* pp. 2165, 2018. DOI: 10.1021/acs.iecr.7b03514.

[39] W. L. Luyben, "Design and Control of a Methanol Reactor/Column Process," *Ind. Eng. Chem. Res.,* vol. 49, *(13),* pp. 6150, 2010. DOI: 10.1021/ie100323d.

[40] A. Valtz *et al*, "Vapour–liquid equilibria in the carbon dioxide–water system, measurement and modelling from 278.2 to 318.2K," *Fluid Phase Equilibria,* vol. 226, pp. 333, 2004. DOI: 10.1016/j.fluid.2004.10.013.

[41] J. A. Herron and C. T. Maravelias, "Assessment of Solar-to-Fuels Strategies: Photocatalysis and Electrocatalytic Reduction," *Energy Tech,* vol. 4, *(11),* pp. 1369, 2016. DOI: 10.1002/ente.201600163.

[42] O. K. M. Fauzan *et al*, "Reducing Energy Consumption in the Formaldehyde Production Process," *Journal of Chemical Engineering Research Progress,* vol. 2, *(1),* pp. 32–40, 2025. DOI: 10.9767/jcerp.20308.

[43] S. A. R. K. Deshmukh, M. V. S. Annaland and J. A. M. Kuipers, "Kinetics of the partial oxidation of methanol over a Fe-Mo catalyst," *Applied Catalysis A: General,* vol. 289, *(2),* pp. 240, 2005. DOI: 10.1016/j.apcata.2005.05.005.

[44] A. Al Matar, "Selecting Fluid Packages (Thermodynamic Model) for HYSYS/ Aspen Plus/ ChemCAD Process Simulators," 2015. DOI: 10.13140/RG.2.1.3461.4487.

[45] J. Thrane *et al*, "A Review and Experimental Revisit of Alternative Catalysts for Selective Oxidation of Methanol to Formaldehyde," *Catalysts,* vol. 11, *(11),* 2021. DOI: 10.3390/catal11111329.

[46] P. Tontiwachwuthikul, A. Meisenz and C. J. Lim, "COz ABSORPTION BY NaOH, MONOETHANOLAMINE AND 2-AMINO-2-METHYL-l-PROPANOL SOLUTIONS IN A PACKED COLUMN+," . DOI: https://doi.org/10.1016/0009-2509(92)80028-B.

[47] Icarus, "Icarus Technology," 1998. DOI: https://www.scribd.com/document/422172125/ICARUS-Reference.

[48] G. T. Rochelle *et al*, "Thermal degradation of amines for CO2 capture," *Current Opinion in Chemical Engineering,* vol. 1, *(2),* pp. 183, 2012. DOI: 10.1016/j.coche.2012.02.004.

[49] Thunder Said Energy. *CCS: what CO2 purity for transport and disposal.* DOI: https://thundersaidenergy.com/downloads/ccs-what-co2-purity-for-transport-and-disposal/#:~:text=The%20minimum%20CO2%20purity%20for%20CCS%20starts,and%20CO2%20liquefaction%20or%20shipping%20requires%20%3E99%.&text=CO2%20purity%20for%20CCS%20will%20generally%20need,ideally%20will%20be%20as%20high%20as%20possible.

[50] M. Mostafa *et al*, "Capturing CO2 from the atmosphere: Design and analysis of a large-scale DAC facility," *Carbon Capture Science &Amp; Technology,* vol. 4, 2022. DOI: 10.1016/j.ccst.2022.100060.

[51] Z. Zolfaghari *et al*, "Simulation of carbon dioxide direct air capture plant using potassium hydroxide aqueous Solution: Energy optimization and CO2 purity enhancement," *Energy Conversion and Management: X,* vol. 21, 2023. DOI: 10.1016/j.ecmx.2023.100489.

[52] R. Turton *et al*, *Analysis, Synthesis, and Design of Chemical Processes.* (Fifth edition ed.) 2022. DOI: https://www.vlebooks.com/vleweb/product/openreader?id=none&isbn=9780134177489.

[53] G. Towler and R. Sinnott, *Principles, Practice and Economics of Plant and Process Design.* 2008.

[54] M. Jouny, W. Luc and F. Jiao, "General Techno-Economic Analysis of CO2 Electrolysis Systems," *Ind. Eng. Chem. Res.,* vol. 57, *(6),* pp. 2165, 2018. DOI: 10.1021/acs.iecr.7b03514.

[55] Lily Lee. *Best Price Iron Drum Packaging Molybdenum Iron Reliable and Good Molybdenum 55~60% Ferro Molybdenum Catalyst*. DOI: https://wxhuanjiang.en.made-in-china.com/product/cFwTDWhoQBYO/China-Best-Price-Iron-Drum-Packaging-Molybdenum-Iron-Reliable-and-Good-Molybdenum-55-60-Ferro-Molybdenum-Catalyst.html?pv_id=1ihqgpfke422&faw_id=1ihqgpng547f.

[56] Imarc, "Carbon Dioxide Pricing Report 2024: Price Trend, Chart, Market Analysis, News, Demand, Historical and Forecast Data," 2024. DOI: https://www.imarcgroup.com/carbon-dioxide-pricing-report.

[57] Mike, "Monoethanolamine price index," 2025. DOI: https://businessanalytiq.com/procurementanalytics/index/monoethanolamine-price-index/.

[58] Mike, "Sodium hydroxide price index," 2025. DOI: https://businessanalytiq.com/procurementanalytics/index/sodium-hydroxide-price-index/.

[59] Mike. (Apr). *Calcium Carbonate Price Index*. DOI: https://businessanalytiq.com/procurementanalytics/index/calcium-carbonate-price-index/.

[60] Mike, "Methanol Price Index," 2025. DOI: https://businessanalytiq.com/procurementanalytics/index/methanol-price-index/.

[61] Ship & Bunker News Team, "Methanol Bunker Demand to Receive Boost From EU Regulations," 2024. DOI: https://shipandbunker.com/news/world/896132-methanol-bunker-demand-to-receive-boost-from-eu-regulations.

[62] Mike, "Formaldehyde price index," 2025. DOI: https://businessanalytiq.com/procurementanalytics/index/formaldehyde-price-index/.

[63] ChemicalBook. (Mar). *Ferric Molybdate*. DOI: https://www.chemicalbook.com/ProductDetail_EN_ferric-molybdate_2332104.htm.

[64] K. V. Raun *et al*, "Deactivation behavior of an iron-molybdate catalyst during selective oxidation of methanol to formaldehyde," *Catalysis Science & Technology,* vol. 8, *(18),* pp. 4626–4637, 2018. DOI: https://www.proquest.com/docview/2108087423. DOI: 10.1039/C8CY01109E.

[65] C. Brookes *et al*, "The Nature of the Molybdenum Surface in Iron Molybdate. The Active Phase in Selective Methanol Oxidation," *J. Phys. Chem. C,* vol. 118, *(45),* pp. 26155, 2014. DOI: 10.1021/jp5081753.

[66] A. P. V. Soares, M. F. Portela and A. Kiennemann, "Methanol Selective Oxidation to Formaldehyde over Iron-Molybdate Catalysts," *Catalysis Reviews,* vol. 47, *(1),* pp. 125, 2007. DOI: 10.1081/cr-200049088.

[67] K. V. Thesis and Raun, "Understanding the Deactivation of the Iron Molybdate Catalyst and its Influence on the Formox Process," Technical University of Denmark. 2018.

[68] L. Sørensen *et al*, "Preliminary Studies into the Environmental Fate of Nitrosamine and Nitramine Compounds in Aquatic Systems," *Energy Procedia,* vol. 37, pp. 683, 2013. DOI: 10.1016/j.egypro.2013.05.157.

[69] I. M. Saeed *et al*, "Opportunities and challenges in the development of monoethanolamine and its blends for post-combustion CO2 capture," *International Journal of Greenhouse Gas Control,* vol. 79, pp. 212, 2018. DOI: 10.1016/j.ijggc.2018.11.002.

[70] K. Zoannou, D. J. Sapsford and A. J. Griffiths, "Thermal degradation of monoethanolamine and its effect on CO2 capture capacity," *International Journal of Greenhouse Gas Control,* vol. 17, pp. 423, 2013. DOI: 10.1016/j.ijggc.2013.05.026.

[71] A. S. Hukkerikar *et al*, "Group-contribution+ (GC+) based estimation of properties of pure components: Improved property estimation and uncertainty analysis," *Fluid Phase Equilibria,* vol. 321, pp. 25, 2012. DOI: 10.1016/j.fluid.2012.02.010.

[72] Y. S. Lee *et al*, "A comparative study of multi-objective optimization methodologies for molecular and process design," *Computers &Amp; Chemical Engineering,* vol. 136, 2020. DOI: 10.1016/j.compchemeng.2020.106802.

[73] B. Kjærside Storm, "12 - surface protection and coatings for wind turbine rotor blades," in *Advances in Wind Turbine Blade Design and Materials*Anonymous 2013, DOI: 10.1533/9780857097286.3.387.

[74] A. V. Rayer, A. Henni and P. Tontiwachwuthikul, "Molar heat capacities of solvents used in CO2 capture: A group additivity and molecular connectivity analysis," *Can J Chem Eng,* vol. 90, *(2),* pp. 367, 2011. DOI: 10.1002/cjce.20646.

[75] O. Odele and S. Macchietto, "Computer Aided Molecular Design: A Novel Method for Optimal Solvent Selection," 1993.

[76] K. Xin, F. Gallucci and M. V. S. Annaland, "Optimization of solvent properties for post-combustion CO2 capture using process simulation," *International Journal of Greenhouse Gas Control,* vol. 99, 2020. DOI: 10.1016/j.ijggc.2020.103080.

[77] B. Yuan *et al*, "Intrinsic insight of energy-efficiency optimization for CO2 capture by amine-based solvent: effect of mass transfer and solvent regeneration," *International Journal of Greenhouse Gas Control,* vol. 118, 2022. DOI: 10.1016/j.ijggc.2022.103673.

[78] R. Carr, P. Guerette and M. James, "Mixed-integer cuts," 2020. DOI: https://optimization.cbe.cornell.edu/index.php?title=Mixed-integer_cuts#:~:text=These%20cuts%20reduce%20the%20feasible,region%20are%20integers%20(3).

[79] F. Ramondo and S. Di Muzio, "Reaction Mechanism of CO2 with Choline-Amino Acid Ionic Liquids: A Computational Study," *Entropy,* vol. 24, *(11),* 2022. DOI: 10.3390/e24111572.

[80] G. Gao *et al*, "Novel assessment of highly efficient polyamines for post-combustion CO2 capture: Absorption heat, reaction rate, CO2 cyclic capacity, and phase change behavior," *Separation and Purification Technology,* vol. 306, 2022. DOI: 10.1016/j.seppur.2022.122615.

[81] H. Yamada *et al*, "Computational investigation of carbon dioxide absorption in alkanolamine solutions," *J Mol Model,* vol. 19, *(10),* pp. 4147, 2013. DOI: 10.1007/s00894-012-1749-9.

[82] J. Clark *et al*. *7.8: Electrophilic Addition Reactions of Alkenes*. DOI: https://chem.libretexts.org/Bookshelves/Organic_Chemistry/Organic_Chemistry_(Morsch_et_al.)/07:_Alkenes-_Structure_and_Reactivity/7.08:_Electrophilic_Addition_Reactions_of_Alkenes.

[83] PWC. (Feb). *Belgium Corporate - Taxes on corporate income*. DOI: https://taxsummaries.pwc.com/belgium/corporate/taxes-on-corporate-income.

[84] Pre-sustainability. (Aug). *ReCiPe*. DOI: https://pre-sustainability.com/articles/recipe/.

[85] Leila *et al*, "Life Cycle Assessment of The Formalin Production Process Using Methods Eco-indicator 99, IMPACT 2002+, EDIP 2003," 2023. DOI: 10.22059/JCHPE.2024.365743.1453.

[86] A. Myat *et al*, "Life Cycle Assessment on Methanol, Dimethyl Ether and Formaldehyde Production for Sustainable Carbon Dioxide Utilization Options," *IJESD,* 2024. DOI: 10.18178/ijesd.2024.15.5.1493.

[87] Mærsk Mc-Kinney, Møller Center. *e-methanol*. 2025. DOI: https://www.zerocarbonshipping.com/energy-carriers/e-methanol/?section=feedstock-availability.

[88] Eurostat. (Sep). *Electricity produced in the EU: 9% based on lignite*. 2020. DOI: https://ec.europa.eu/eurostat/web/products-eurostat-news/-/ddn-20200914-1#:~:text=Nine%20Member%20States%20in%20the%20European%20Union,'brown%20coal'%2C%20for%20electricity%20and%20heat%20production.&text=In%202018%2C%209%%20of%20total%20gross%20electricity,than%20double%20the%20amount%20from%20solar%20photovoltaic..

[89] G. Garcia *et al*, "Analytical Review of Life-Cycle Environmental Impacts of Carbon Capture and Utilization Technologies," *ChemSusChem,* vol. 14, pp. 995, 2021. DOI: 10.1002/cssc.202002126.

[90] Reuters, "SWECO: Sweco to design one of Europe's largest battery energy storage systems in Belgium," *Reuters,* 2024. DOI: https://www.reuters.com/business/energy/sweco-design-one-europes-largest-battery-energy-storage-systems-belgium-2024-10-07/.